Journal of Materials Chemistry B

RSC Publishing

PAPER

View Article Online
View Journal | View Issue

Cite this: J. Mater. Chem. B, 2013, 1, 2943

Monetite promoting effect of NaCl on brushite cement setting kinetics

Erdem Şahin* and Muhsin Çiftçioğlu

Received 28th January 2013
Accepted 11th April 2013

DOI: 10.1039/c3tb20130a

www.rsc.org/MaterialsB

Brushite forming calcium phosphate cements (CPCs) have received growing interest for scaffold applications due to their high surface area and high bioresorbability. The dehydrated form of brushite, monetite, has a finer microstructure with higher surface area, higher strength and bioresorbability comparable to brushite, making it a viable alternative phase in CPCs. The increase in monetite content of the β-tricalcium phosphate (β-TCP)–monocalcium phosphate monohydrate (MCPM) cement system due to the reduction in its supersaturation upon addition of NaCl to excess setting liquid was investigated kinetically. The relaxation period was monitored by pH-stat titration of the cement solution by 0.1 M NaOH. Monetite growth was achieved in shorter periods at higher NaCl concentrations where the supersaturation gap between brushite and monetite is thought to be narrowed due to high ionic strength in accord with Pitzer's ion interaction model. The brushite/monetite ratio decreased consistently with increasing NaCl concentration in the 3–6 M range.

Introduction

Calcium phosphate cements (CPCs) were discovered by LeGeros, Brown and Chow in the 1980s as alternative materials to bulky bone graft bioceramics that set *in situ* and fill bone or dental defects. CPCs set and harden essentially *via* an acid–base reaction involving dissolution and precipitation. According to Chow, the discovery of the first CPC was in fact a result of decades of basic studies on calcium phosphate solubility behavior.[1] CPCs are made by mixing an aqueous solution with one or several calcium phosphate powders. Relatively soluble calcium phosphates dissolve and precipitate into a less soluble calcium phosphate phase upon mixing with water. Dissolution of the reactants supplies calcium and phosphate ions to the solution, while formation of the stable phase depletes these ions. Calcium phosphate crystals intergrow during the setting stage and provide a mechanical rigidity to the cement.

Brushite cements, although mechanically weaker than apatite cements, have received growing interest as bone graft materials for the utilization of their high bioresorbability.[2–4] Brushite, the main phase of conventional brushite cement, displays the smooth plate-like crystal morphology. Its more stable, anhydrous form monetite crystallizes in a finer stacked-sheet structure with specific surface area approaching nanosize hydroxyapatite depending on the processing conditions.[5,6] Its reported higher mechanical properties stem from the finer microstructure.[7,8] Transformation of brushite to monetite is accompanied by micropore formation as a result of water exclusion.[9–12] Monetite transformation by various methods was reported in the literature including heat treatment,[10–12] utilization of impurities,[9,13] and use of excess acidic precursors[8,14] in which control on the extent of phase transformation and micropore formation was absent.

It has been shown in many studies on phase transformations in calcium phosphate solutions[15–18] that the thermodynamically stable phase eventually forms but the precipitation order is determined by kinetics according to the Ostwald rule of stages. Ostwald states that kinetic, not thermodynamic properties of the calcium phosphate phases determine the rate and order of appearance of intermediate phases.[4] Brushite forming calcium phosphate cement sets in accord with this law so that an energetically favorable brushite phase forms rather than a thermodynamically stable monetite phase that is more supersaturated.

Among the factors directly affecting the formation order and driving force of the stable calcium phosphate phases, the most prominent effect is caused by the ionic strength of the cement setting liquid as demonstrated in Fig. 1 by the highly precise Pitzer model of ionic activity in electrolyte solutions. With the assumption of equal calcium and phosphate ion concentrations in brushite cement setting liquid, both supersaturations of brushite and monetite and the difference between their supersaturations exponentially decrease with increasing ionic strength of the solution.

The ion-specific interaction equation developed by Pitzer for complex electrolyte solutions is an expansion of the Debye–Huckel equation and is valid up to 6 M.[19] Ion interaction parameters are determined from single electrolyte solutions and

Department of Chemical Engineering, İzmir Institute of Technology, Turkey. E-mail: erdemsahin@iyte.edu.tr; muhsinciftcioglu@iyte.edu.tr; Fax: +90 2327506645; Tel: +90 2327506645; +90 2327506669

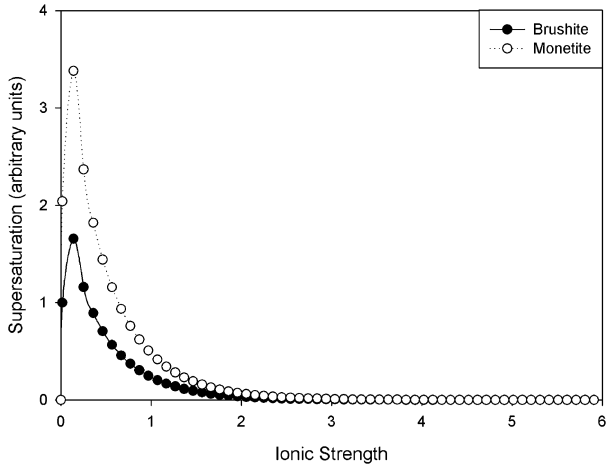

Fig. 1 Supersaturation of brushite and monetite in the presence of NaCl as predicted by the Pitzer equation.

from mixed solutions with either a common cation or anion. The constants used in the calculation of the supersaturation for calcium phosphates are given by Pitzer and colleagues.[20–23] NaCl is soluble in water at 25 °C up to 6.143 M. Pitzer's equation predicts the supersaturation of calcium phosphates accurately in a wide range of NaCl concentrations from 0 to about 6 M. Supersaturations of both brushite and monetite are suppressed to extremely low values around an ionic strength of 3 as seen in Fig. 1. Theoretically, addition of about 3 M NaCl is sufficient to reduce the supersaturation of calcium phosphates to such low levels that surface integration of ions is expected to become the rate determining step of crystallization. According to Mersmann, crystal growth is controlled by diffusion at high supersaturations and low solubility.[24]

The role of NaCl as an ionic modifier in the reduction of the supersaturation was investigated in this study and it was utilized as a control parameter for monetite formation. High supersaturations encountered at low ionic modifier concentrations are expected to result in high crystal growth rates. Dissolution of cement precursors on the other hand is expected to be hindered at high ionic strength, further lowering the driving force for crystallization. Growth curves of the conventional brushite cement system set in excess aqueous solution containing NaCl were analyzed in order to determine their effect on monetite phase formation despite the unfavorable kinetic conditions for crystal growth. The results of the study will provide cues for controlling monetite content in acidic cement setting applications under sufficiently high crystal growth rates.

Experimental

The setting kinetics of the β-TCP–MCPM cement system was analyzed using a potentiometric titrator (Kyoto Electronic AT-510) to measure the base uptake as the extent of growth at a fixed pH value of 4.2. This value was chosen for its proximity to 4.3 which is the singular point between monetite and hydroxyapatite to prevent any hydroxyapatite formation. The observable effects of the ionic modifier NaCl on the kinetics of the cement setting reaction were isolated by keeping other kinetic factors constant. Introduction of seeds reduced the supersaturation build-up so that precipitates formed close to equilibrium conditions. Eliminating variations in temperature and pH also made it possible to investigate the effects of ionic modifiers on the relaxation period at various concentrations.

The effect of ionic strength on the setting reaction of stoichiometric cement formulation was investigated by adding NaCl to the setting liquid of the powder mixture. The mixture consisted of 1.55 gr β-TCP, 1.26 gr MCPM and 0.1 gr brushite seed. β-TCP (Sigma 21218) and MCPM (Sigma C8017) precursor powders had median particle sizes (d_{50}) of 5.5 μm and 33 μm, respectively. NaCl (Merck 106404) concentration in 100 ml of deionized water varied in the ranges of 1–6 M. 0.1 M NaOH (Sigma 221465) was used as titration base. Variations in base uptake and the pH were recorded as a function of time for the observable period of 9999 seconds. Precipitation products were centrifuged, frozen and freeze-dried in order to investigate the microstructure by XRD, SEM and EDX analysis. Free-drift runs in addition were conducted under similar conditions in order to observe the variation in pH as an indication of CPC growth.

XRD analysis was conducted by using a Philips X'Pert Pro powder diffractometer with Cu K_α radiation at a generator voltage of 45 kV and a tube current of 40 mA. All XRD patterns were obtained at a scan range of 5–60° and a scan step size of 0.05 and 5 seconds per step. The external standard method was employed for the semi-quantitative XRD analysis. The relative intensity ratio of the constituent phases with respect to the external standard corundum was obtained by measurement of the ratio of the intensities of the characteristic peaks to intensities of the characteristic peaks of the corundum. Powder mixtures of pure constituent phases and corundum were prepared at a 1 : 1 weight ratio. The XRD patterns of the mixtures were resolved for the intensity of the three characteristic peaks of each phase. The mass absorption coefficients of calcium phosphate phases were obtained from the literature.[25] Characteristic peaks of constituent phases separated by a minimum angle of 1 degree were used to characterize the phase composition of the samples by measurement of the net peak intensities. Obtained intensities, relative intensity ratio, and mass absorption coefficients were inserted into the governing external standard method equation to obtain weight ratios:[26]

$$W_a = \left[\frac{I_a^{hkl}}{I_a^{REL}}\right]\left[\frac{(\mu/\rho)_m}{(\mu/\rho)_s}\right]\left[\frac{1}{I_s^p RIR_a}\right] \quad (1)$$

where I_a^{hkl} is the intensity of the (hkl) peak of phase α, I_a^{REL} is the relative intensity of the (hkl) peak with respect to other peaks of the same phase, $(\mu/\rho)_m$ is the mass absorption coefficient of the mixture, $(\mu/\rho)_s$ is the mass absorption coefficient of the reference standard, RIR_a is the relative intensity ratio of phase α with respect to the reference standard, and I_s is the intensity of the 100% peak of the reference standard phase s, taken by convention to be α-Al_2O_3, corundum.

Besides the expected β-TCP (JCPDS# 09-0169), brushite (JCPDS# 72-0713) and monetite (JCPDS# 77-0128) phases, additional phases were observed including NaCl (JCPDS# 05-0628) and sodium calcium phosphate (JCPDS# 29-1193).

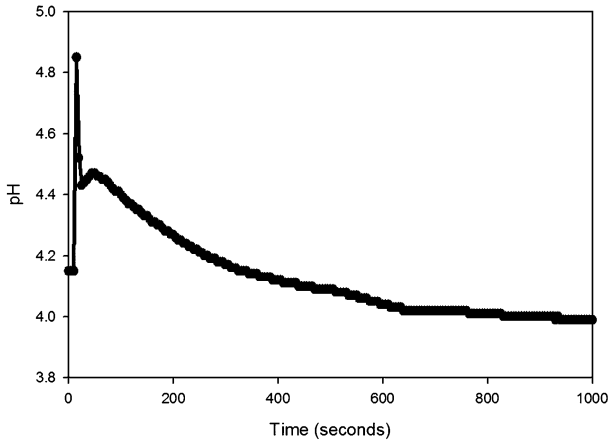

Fig. 2 Variation in the pH of the setting solution for β-TCP–MCPM cement with brushite seeds.

A significant amount of NaCl was formed during the centrifugal separation of the precipitates from the setting liquid. Its quantity was calculated with the corresponding RIR values and subtracted from the total concentration. The remaining weight percent values were totaled up to 100%.

Morphological analysis was done by using a Philips XL-30S FEG scanning electron microscope. A secondary electron detector was used to capture micrographs at an accelerating voltage of 5.00 kV and a wedge distance of 10 mm. An electron dispersive X-ray detector was used for elemental analysis of the sample surface.

Results and discussion

Upon mixing the cement precursors with excess setting liquid, MCPM instantly dissolves and supplies $H_2PO_4^-$ and Ca^{2+} ions to the solution. A small fraction of $H_2PO_4^-$ is expected to dissociate into H^+ and HPO_4^{2-} ions due to its relative stability among phosphoric acid species in water at room temperature.[27] β-TCP dissolves simultaneously to release $3Ca^{2+}$ and $2PO_4^{3-}$ that can form brushite $CaHPO_4 \cdot 2H_2O$ provided that the same amount of H^+ ions are removed from the solution to first form HPO_4^{2-} groups, resulting in an initial increase in solution pH as seen in Fig. 2. The H^+ ions supplied by $H_2PO_4^-$ ions are expected to increase over time as more H^+ ions are consumed by dissolving β-TCP species and a net decrease in pH is expected as growth progresses shortly after mixing the reactant with water. Built-up supersaturation is quickly relaxed in the system under study due to the presence of brushite seeds as brushite is known to be preferred to monetite at pH 4.2 and room temperature.[28] The local maximum observed in Fig. 2 around 100 seconds is an indication of the supersaturation build-up due to fast β-TCP dissolution at lower pH and the subsequent gradual pH fall indicates that brushite growth has speeded up relative to β-TCP dissolution. Precipitation and β-TCP dissolution act to balance the supersaturation and pH until the rate of one weakens relative to the other.[29] This interplay between dissolution and precipitation continues indefinitely until the consumption of precursors.

Brushite cement set in pure water under ambient conditions to form brushite as the main end product. XRD patterns of brushite cement set in excess pure water given in Fig. 3 show no trace of MCPM but a significant amount of β-TCP residue. MCPM completely dissolves upon mixing with water while β-TCP dissolution continues indefinitely as explained in the above discussion. Phase analysis of precipitates obtained in the titration runs indicates the changes in the growth mechanism and kinetics of the system. For instance, the weakening of brushite peaks upon addition of 3 and 6 M NaCl that is visible in XRD patterns given in Fig. 3 suggests that monetite is kinetically favored at the early stages of setting by the increase in ionic strength.

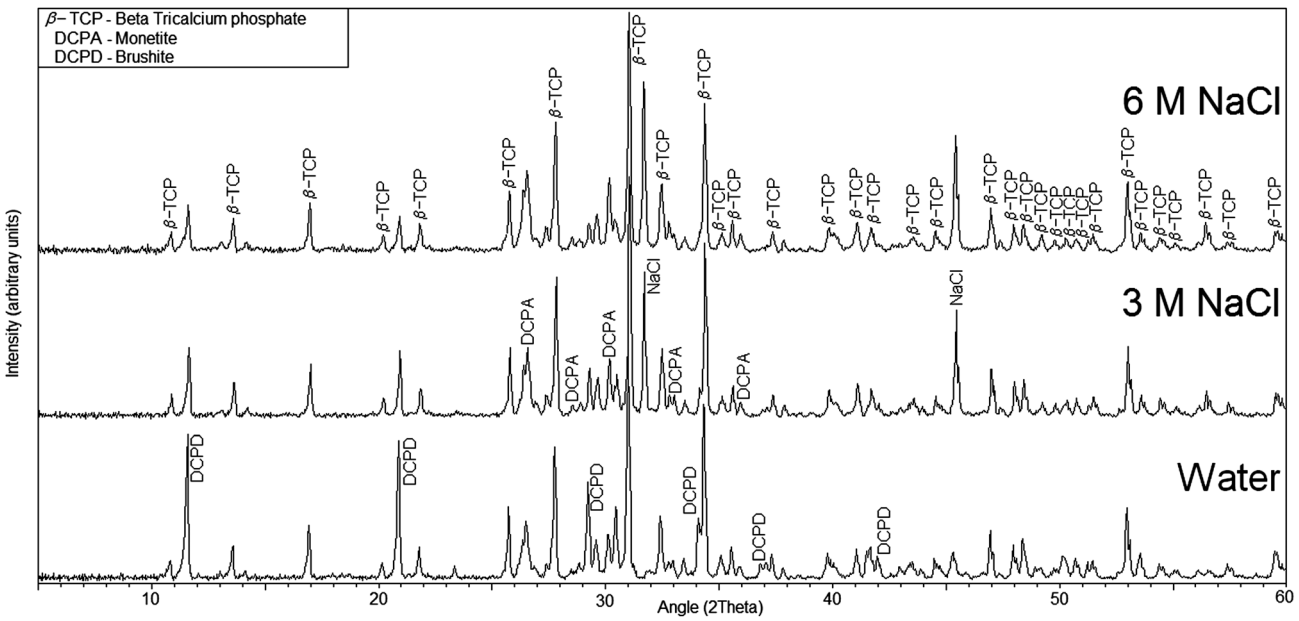

Fig. 3 XRD patterns of precipitates obtained from cement setting in pure water, 3 M NaCl and 6 M NaCl solutions.

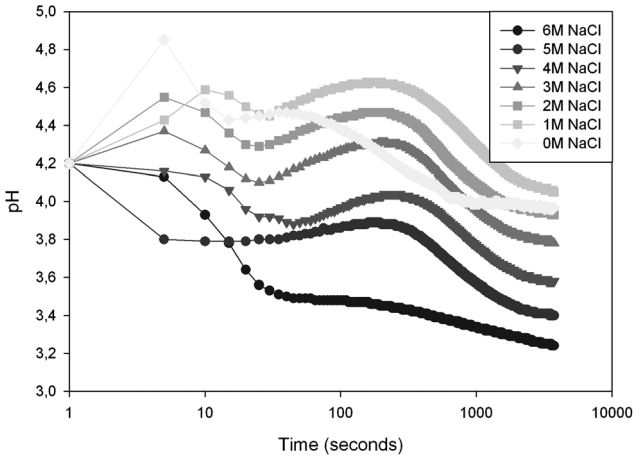

Fig. 4 Variation in the pH of the setting solution for β-TCP–MCPM cement in free drift runs with increasing NaCl concentration.

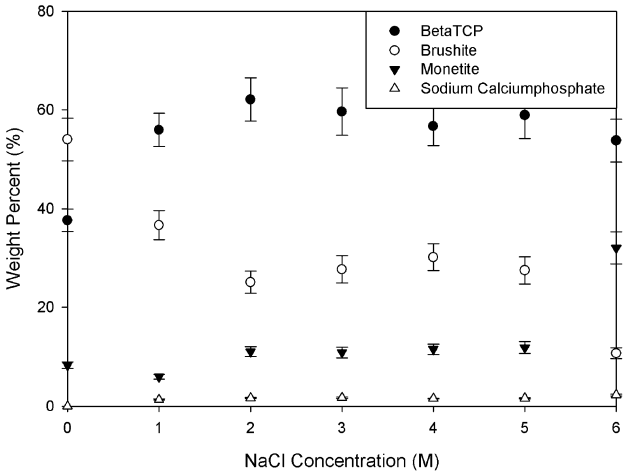

Fig. 5 Phase composition of samples from free drift in liquid containing various NaCl concentrations.

Free drift runs

NaCl was introduced into 100 mL of setting liquid up to 6 M concentration. Free drift and pH-stat monitoring of β-TCP–MCPM cement in the presence of 3% seed were conducted at ambient temperature. The initial sharp peak corresponding to simultaneous dissolution of MCPM and β-TCP diminished gradually with increasing NaCl concentration as seen in Fig. 4. Increasing the NaCl concentration shifted the instantaneous pH of the setting liquid to a lower value, by about $\Delta pH = 0.2$ with each 1 M increase. The pH drop observed with increasing NaCl concentration was a result of dissociation of $H_2PO_4^-$ into HPO_4^{2-} and H^+ in the absence of the H^+ consuming PO_4^{3-} ions that dissociate from β-TCP. The supersaturation build-up represented by the broad peak also occurred later compared to pure water and a higher peak was observed for lower NaCl concentrations. The height and slope of the broad peak decreased with increasing NaCl concentration up to 6 M where supersaturation build-up was finally not detected due to effective suppression of β-TCP dissolution at the highest ionic strength attained. This is also attributed to the decrease in solubility of the calcium source β-TCP as sodium, a monovalent cation, is expected to decrease the equilibrium concentration of cations with similar electron affinity.[30]

The phase composition of free drift samples given in Fig. 5 reveals that NaCl addition inhibited β-TCP dissolution remarkably despite the observed pH drop. Brushite amount decreased and monetite amount increased especially at low (1–2 M) and high (5–6 M) NaCl concentrations. A slight increase in brushite amount was detected around 3 M NaCl where the growth kinetics is thought to be dominated by diffusion as the initial pH rise of the solution diminished and β-TCP dissolution is enhanced. A further change in growth kinetics may be responsible for the inhibition of brushite growth encountered above 5 M NaCl as diffusion is also slowed down by the suppressed solubility of β-TCP at high ionic strengths. Although both diffusion and surface integration are expected to slow down at high NaCl concentrations, only the brushite amount is seen to decrease for the two cement end products. Monetite formation was positively affected by the changes in growth kinetics due to its thermodynamic stability at low pH attained by increasing NaCl concentration.

pH-stat runs

The pH-stat instrument used in this work is responsive when the pH drops below 4.2 and did not track the pH fluctuations in the initial dissolution lag-time period. The recorded data contain kinetic information about growth on the existing brushite seeds after the initial mixing, dissolution and supersaturation build-up periods. Constant pH and constant composition studies on calcium phosphate precipitation conducted by van Kemenade *et al.* successfully demonstrated the order and extent of calcium phosphate formation by analysis of the relaxation curves.[15] The growth curve given in Fig. 6 for CPC set in pure water is a well-defined sigmoidal curve that represents the relaxation period in reverse. The inflection point of the sigmoidal curve represents the point of maximum growth rate and the end plateau indicates the kinetic balance between β-TCP dissolution and brushite growth which occurs when the

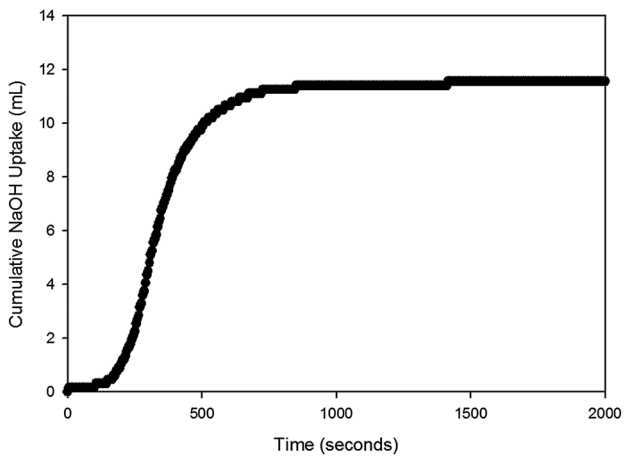

Fig. 6 Cumulative base uptake of β-TCP–MCPM cement with brushite seeds.

concentration of the forming phase is close to saturation. Fig. 7 gives the cumulative base uptake of cement setting in water containing 0 to 6 M NaCl. Pure setting liquid produces a well-defined sigmoidal curve representative of a relaxation period that starts and ends relatively faster than NaCl containing setting liquid up to 3 M NaCl. The addition of small amounts of NaCl extends the relaxation period significantly. The single sigmoidal curves represent brushite and monetite growth based on the quantitative XRD data. Double sigmoidal curves were observed in our current research on the synergistic effect of NaCl and citric acid, the second curve may be attributed solely to monetite formation. Brushite cement setting in the presence of NaCl is retarded by NaCl additions up to 3 M and confined to earlier times upon increasing the NaCl concentration as seen in Fig. 8. The observed variation is parallel to the variation in calcium phosphate supersaturation as predicted by Pitzer's ion interaction model given in Fig. 1 since the crystal growth rate is proportional to supersaturation. The exponential decrease in the difference of supersaturations at high ionic strengths is thought to be the operative mechanism for the suppression in the brushite relaxation period observed in Fig. 8. As a consequence of high ionic strength, the thermodynamic stability of both phases decreases and brushite becomes as stable as monetite which renders brushite kinetically less favorable according to the Ostwald rule of stages.

An increase in the setting times of cement blocks with increasing NaCl concentration is reported in the study by Cama *et al.* on the utilization of NaCl for macroporous monetite scaffold synthesis.[31] The mechanical properties of cement blocks are parallel to the setting extent[32] and NaCl is seen to modify the setting order as well as the setting extent. The shift in the maximum growth rates to earlier periods in the present study indicates the inhibition of brushite setting rather than the setting extent. In fact, low cement growth rates in excess setting liquid results in a low degree of setting as evident from the phase compositions given in Fig. 5.

Sigmoidal curves observed in Fig. 7 were curves fitted to perfect sigmoids and their derivatives were taken in order to obtain the variation of growth rate as a function of time. As seen in the growth rate curves given in Fig. 9, the peak rates corresponding to the inflection points of the sigmoidal curves shift to lower times with increasing NaCl concentration. The areas under the rate curves give the total base uptake at infinite time. Equal values of total base uptake for all concentrations of NaCl confirm that the main effect of NaCl shifts the maximum growth rates to early times within the observed experiment period. Compression of the growth period with increasing NaCl concentration is attributed to the increasingly rapid consumption of HPO_4^{2-} ions supplied by stable $H_2PO_4^-$ groups as a result of the exponential decrease in their supersaturation as predicted in Fig. 1. Constituent ions of brushite and monetite are expected to be integrated rapidly to crystal surfaces without a need for supersaturation build up at high ionic strengths attained.

Calcium and phosphate ions are depleted quickly at high NaCl concentrations due to their depressed activity and the sudden formation of the growing phases as evident from the sharper sigmoidal curves in Fig. 9. The supersaturation build-up and relaxation periods are compressed with increasing NaCl concentrations and a change in growth model is thought to occur from diffusion controlled to surface integration controlled around 3 M NaCl. It is seen in Fig. 10 that brushite

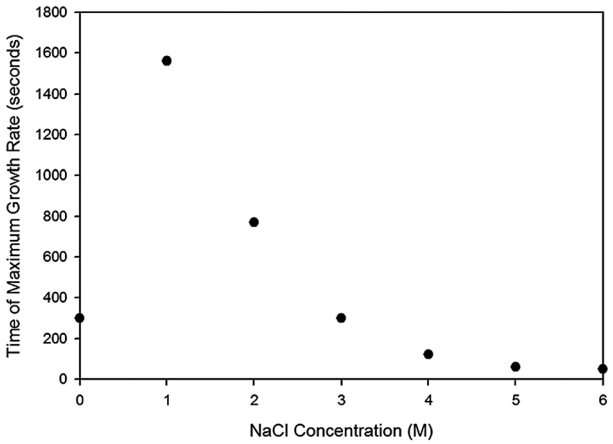

Fig. 8 Variation in time of maximum growth rate with NaCl concentration close to saturation.

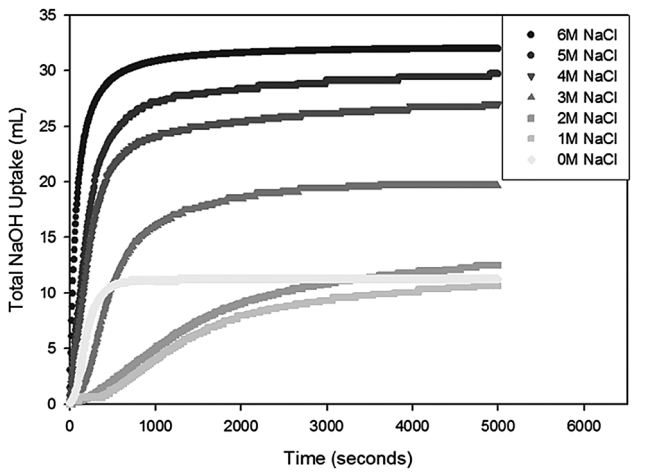

Fig. 7 Cumulative base uptake curves for cement setting with various NaCl concentrations.

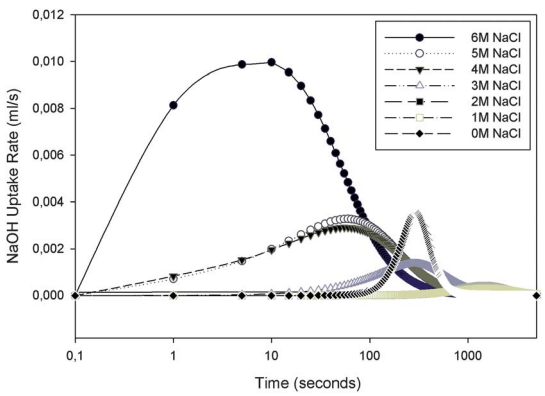

Fig. 9 Variation of growth rates with increasing NaCl concentration.

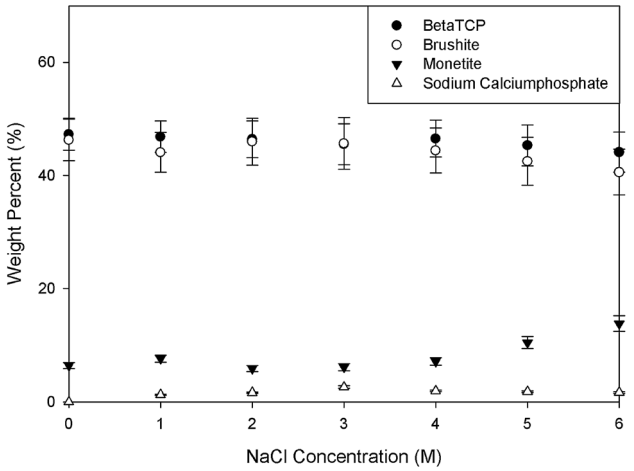

Fig. 10 Phase composition of calcium phosphate cement set in the presence of varying NaCl concentration.

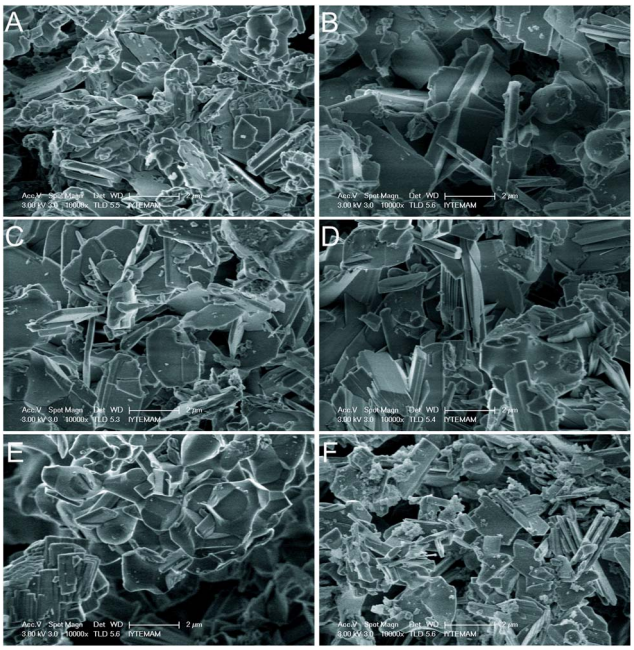

Fig. 11 Crystal morphology of samples set in 1–6 M NaCl aqueous solution at constant pH and temperature. (A) 1 M NaCl, (B) 2 M NaCl, (C) 3 M NaCl, (D) 4 M NaCl, (E) 5 M NaCl, and (F) 6 M NaCl.

and monetite are present in all NaCl concentrations and the brushite/monetite ratio starts to decrease consistently with increasing NaCl concentration above 3 M NaCl. This may be attributed to the drop of pH observed in the free drift runs as a result of $H_2PO_4^-$ dissociation into HPO_4^{2-} and H^+. The equilibrium pH of the NaCl containing setting liquids drops below 4.2 at 3 M NaCl as seen in Fig. 4.

Whether the observed change in the brushite/monetite ratio is due to ionic strength or initial drop in pH can be resolved by comparing the phase composition of the pH-stat runs and free drift runs where pH was allowed to decrease throughout setting. While lower pH values in free drift runs favored monetite rather than brushite, the increase in monetite content relative to brushite for the constant pH runs similar to that in Fig. 5 reveals that high ionic strength is effective in the suppression of supersaturation. The overall higher brushite content observed in pH-stat runs compared to the free drift runs with lower pH shows that brushite is favored relative to monetite at higher pH as reported in the literature.[8]

Cama *et al.* bring alternative views to the discussion such that the monetite promoting effect of NaCl is attributed to many reasons.[31] The authors based on their calorimetric studies show that the rate of the exothermic reaction was higher in the absence of sodium chloride. The authors further discuss that substitution of Na^+ ions in the precursor crystal structure may adversely affect the dissolution of β-TCP and hence change the setting kinetics. The most likely reason for promotion of monetite content among the proposed theories is the pH reduction in the setting liquid in the presence of NaCl. The liquid volume is quite low at a powder/liquid ratio of 3 used in the preparation of monetite cement blocks. A decrease in the dissolution rate of both precursors at high ionic strength coupled with low water volume should result in a gradual decrease in solution pH parallel to the slow dissolution of undersaturated MCPM.

Phase evolution of the cement samples with increasing NaCl concentration is exhibited in the SEM images given in Fig. 11. The majority of the observed crystals are identified as smooth brushite (010) plates elongated in the planar [110] direction. The crystal structure consists of two parallel layers that are composed of sheets of calcium phosphate molecules and water molecules.[33] The hydrate layer that is present on the surface of the crystals in aqueous solutions is responsible for the observed smoothness of brushite crystals. Crystal sizes remain in a few micrometers range throughout all solution concentrations. Round β-TCP crystals are mostly hidden in the background and only the precipitated crystals reside on the surface of the samples. Smooth, rigid brushite plates are seen to evolve into the stacked sheet-like structure that is characteristic of monetite crystals at high ionic strengths as evident in Fig. 11E and F. Monetite crystal structure is free from the hydrate layer and the stacked sheet-like $CaHPO_4$ chains are bonded together by Ca–O bonds and three types of hydrogen bonds.[34]

Atomic percentages of the constituent elements Ca, P and O determined *via* energy dispersive X-ray analysis were compared to the elemental ratio deduced from the X-ray diffraction quantitative phase analysis. The results shown in Table 1 are in close agreement except the small deviation in especially P content. The mismatch is due to experimental restrictions as some β-TCP was removed from the EDX analyzed sample in the leaching water used in order to remove NaCl. XRD analysis was done in the presence of excess NaCl, the quantity of which was subtracted from the total phase percentage to obtain the calcium phosphate phase composition. The Ca/P ratio around 1.23 for the XRD analyzed samples indicates a higher β-TCP content, while the increase in brushite and monetite content at maximum NaCl concentration is reflected by the decline in the Ca/P ratio.

Monetite formation extent of brushite cement set in excess setting liquid containing various NaCl concentrations is modest

Table 1 Elemental analysis of samples set in 1–6 M NaCl aqueous solution

	EDX							XRD						
NaCl	O%	+/−	P%	+/−	Ca%	+/−	Ca/P	O%	+/−	P%	+/−	Ca%	+/−	Ca/P
1 M	67.25	2.24	15.81	0.76	16.95	0.94	1.07	68.26	4.55	14.16	1.32	17.59	1.41	1.24
2 M	66.75	2.23	15.41	0.66	17.84	0.82	1.16	68.44	4.45	14.09	1.16	17.47	1.34	1.24
3 M	65.92	2.64	15.23	0.56	18.85	0.70	1.24	68.46	3.85	14.11	1.14	17.43	1.41	1.24
4 M	66.72	3.11	15.59	0.83	17.69	1.03	1.13	68.30	4.45	14.15	1.40	17.55	1.59	1.24
5 M	67.29	2.69	15.56	0.77	17.15	0.95	1.10	68.19	3.93	14.25	1.17	17.56	1.29	1.23
6 M	68.00	3.17	15.15	0.72	16.85	0.88	1.11	68.08	3.40	14.35	1.01	17.57	1.12	1.22

compared to clinical cement applications utilizing a low setting liquid volume. The present study provides a baseline for phase composition of brushite cement in order to understand and control the change in the growth kinetics by ionic modification using excess NaCl. The growth rates and hence monetite formation extent are significantly improved under sufficiently high calcium phosphate supersaturations as reported in the literature.[31] Our recent study on the monetite promotion in brushite cement blocks in the presence of NaCl and an adsorbing impurity citric acid reveals that about 85% monetite yield is obtained in cement blocks set in water containing an optimum citric acid and maximum NaCl concentration.[35] The theoretical dense compressive strength of monetite rich cement is seen to reach twice that of brushite cement. Thus it is possible to utilize monetite cements in hard tissue engineering applications with control on phase evolution provided that the accompanying microporosity is minimized.

Conclusions

Experimental verification of Pitzer's ion interaction model on the calcium phosphate cement system was done by a series of kinetic observations reflecting the cement growth kinetics of the β-TCP–MCPM system. The supersaturation gap between the competing stable phases brushite and monetite is the governing factor for the order of precipitation according to the Ostwald rule of stages. The decrease in the calcium and phosphate supersaturations predicted by the model was found to fit the growth kinetics of the cement system. The effect of ionic strength demonstrated by the addition of NaCl to the cement setting liquid was the decrease in growth rates in favor of monetite. Monetite became less thermodynamically stable and more kinetically favorable with increasing ionic strength in brushite cement setting liquid. The effectiveness of NaCl addition to the setting liquid on the order and extent of calcium phosphate cement precipitation was seen to increase at high concentrations near its solubility limit.

Acknowledgements

The authors thank the facility and staff of Izmir Institute of Technology, Biotechnology and Bioengineering Research and Application Center and Materials Research Center for their contribution on the experimental work.

References

1 L. C. Chow, *Dent. Mater. J.*, 2009, **28**, 1–10.
2 L. M. Grover, J. C. Knowles, G. J. Fleming and J. E. Barralet, *Biomaterials*, 2003, **24**, 4133–4141.
3 D. Apelt, F. Theiss, A. O. El-Warrak, K. Zlinszky, R. Bettschart-Wolfisberger, M. Bohner, S. Matter, J. A. Auer and B. von Rechenberg, *Biomaterials*, 2004, **25**, 1439–1451.
4 J. Nyvlt, *Cryst. Res. Technol.*, 1995, **30**, 443–449.
5 Y. Tokudome, A. Miyasaka, K. Nakanishi and T. Hanada, *J. Sol-Gel Sci. Technol.*, 2010, **57**, 269–278.
6 H. Hohl, P. G. Koutsoukos and G. H. Nancollas, *J. Cryst. Growth*, 1982, **57**, 325–335.
7 T. Kodaka and M. Kobori, *J. Electron Microsc.*, 1999, **48**, 167–172.
8 J. Aberg, H. Brisby, H. B. Henriksson, A. Lindahl, P. Thomsen and H. Engqvist, *J. Biomed. Mater. Res., Part B*, 2010, **93**, 436–441.
9 M. H. Alkhraisat, F. T. Marino, C. R. Rodriguez, L. B. Jerez and E. L. Cabarcos, *Acta Biomater.*, 2008, **4**, 664–670.
10 M. Bohner, H. P. Merkle and J. Lemaitre, *J. Mater. Sci.: Mater. Med.*, 2000, **11**, 155–162.
11 L. M. Grover, U. Gbureck, A. M. Young, A. J. Wright and J. E. Barralet, *J. Mater. Chem.*, 2005, **15**, 4955–4962.
12 F. Tamimi, J. Torres, C. Kathan, R. Baca, C. Clemente, L. Blanco and E. Lopez Cabarcos, *J. Biomed. Mater. Res., Part A*, 2008, **87**, 980–985.
13 M. Bohner, H. P. Merkle, P. V. Landuyt, G. Trophardy and J. Lemaitre, *J. Mater. Sci.: Mater. Med.*, 1999, **11**, 111–116.
14 L. G. Galea, M. Bohner, J. Lemaitre, T. Kohler and R. Muller, *Biomaterials*, 2008, **29**, 3400–3407.
15 P. L. de Bruyn and M. J. J. M. van Kemenade, *J. Colloid Interface Sci.*, 1987, **118**(2), 564–585.
16 R. I. Martin and P. W. Brown, *J. Am. Ceram. Soc.*, 1997, **80**, 1263–1266.
17 A. C. Tas and S. B. Bhaduri, *J. Am. Ceram. Soc.*, 2004, **87**, 2195–2200.
18 A. C. Tas, *J. Am. Ceram. Soc.*, 2009, **92**, 2907–2912.
19 R. Sheikholeslami and H. W. K. Ong, *Desalination*, 2003, **157**, 217–234.
20 K. S. Pitzer and G. Mayorga, *J. Phys. Chem.*, 1973, **77**, 2300–2308.
21 K. S. Pitzer and G. Mayorga, *J. Solution Chem.*, 1974, **3**(7), 539–546.
22 B. S. Krumgalz, *J. Mol. Liq.*, 2001, **91**, 3–19.

23 K. S. Pitzer, *J. Phys. Chem.*, 1973, **77**(2), 268–277.
24 A. Mersmann, *Crystallization Technology Handbook*, Marcel-Dekker, Inc., 2001.
25 B. D. Cullity, *Elements of X-Ray Diffraction*, Addison-Wesley, 1956.
26 R. L. Snyder, *Introduction to X-Ray Powder Diffractometry*, Wiley-Interscience, 1996.
27 L. Wang and G. H. Nancollas, *Chem. Rev.*, 2008, **108**, 4628–4669.
28 U. Gbureck, S. Dembski, R. Thull and J. E. Barralet, *Biomaterials*, 2005, **26**, 3691–3697.
29 M. Bohner and U. Gbureck, *J. Biomed. Mater. Res., Part B*, 2008, **84**, 375–385.
30 A. E. König, H. H. Emons and J. Nyvlt, *Cryst. Res. Technol.*, 1987, **22**(1), 13–19.
31 G. Cama, B. Gharibi, M. S. Sait, J. C. Knowles, A. Lagazzo, S. Romeed, L. Di Silvio and S. Deb, *J. Mater. Chem. B*, 2013, **1**, 958–969.
32 E. Fernandez, F. J. Gil, S. M. Best, M. P. Ginebra, F. C. Driessens and J. A. Planell, *J. Biomed. Mater. Res.*, 1998, **41**, 560–567.
33 K. Flade, C. Lau, M. Mertig and W. Pompe, *Chem. Mater.*, 2001, **13**, 3596–3602.
34 L. Tortet, J. R. Gavarri, G. Nihoul and A. J. Dianoux, *J. Solid State Chem.*, 1997, **132**, 6–16.
35 E. Şahin and M. Çiftçioğlu, unpublished work.